analytical chemistry

ACS AUTHORCHOICE

pubs.acs.org/ac Article

Estimating the Reduced Scattering Coefficient of Turbid Media Using Spatially Offset Raman Spectroscopy

Sara Mosca, Priyanka Dey, Marzieh Salimi, Benjamin Gardner, Francesca Palombo, Nick Stone,* and Pavel Matousek*

Cite This: *Anal. Chem.* 2021, 93, 3386−3392 Read Online

ACCESS | Metrics & More | Article Recommendations | Supporting Information

ABSTRACT: We propose a new method for estimating the reduced scattering coefficient, μ_s', of turbid homogeneous samples using Spatially Offset Raman Spectroscopy (SORS). The concept is based around the variation of Raman signal with SORS spatial offset that is strongly μ_s'-dependent, as such, permitting the determination of μ_s'. The evaluation is carried out under the assumptions that absorption is negligible at the laser and Raman wavelengths and μ_s' is approximately the same for those two wavelengths. These conditions are often satisfied for samples analyzed in the NIR region of the spectrum where SORS is traditionally deployed. Through a calibration procedure on a PTFE model sample, it was possible to estimate the μ_s' coefficient of different turbid samples with an error (RMSEP) below 18%. The knowledge of μ_s' in the NIR range is highly valuable for facilitating accurate numerical simulations to optimize illumination and collection geometries in SORS, to derive in-depth information about the properties of SORS measurements or in other photon applications, dependent on photon propagation in turbid media with general impact across fields such as biomedical, pharmaceutical, security, forensic, and cultural sciences.

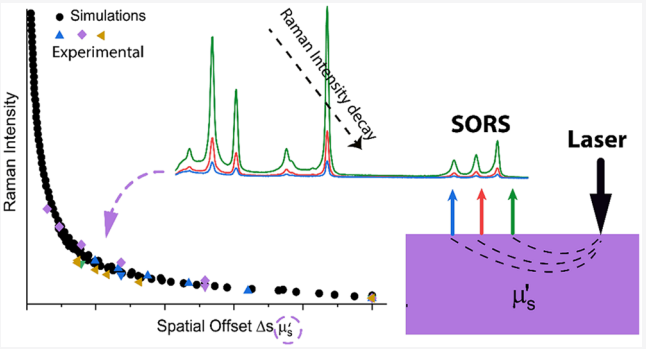

A number of optical analytical techniques are critically dependent on the propagation of light in diffusely scattering media.[1] This process is governed principally by the medium's scattering and absorption coefficients.[2,3] Numerous methods have been proposed and demonstrated in the past to measure these parameters. Many of them are based around measuring the intensity of near-infrared (NIR) light, often in a spectrally resolved manner, that is injected into the sample at a given location with temporal and spatial resolution.[1] In this study, we propose a simple, alternative concept enabling the estimation of the scattering coefficient of homogeneous samples using only Spatially Offset Raman Spectroscopy (SORS) data.[4] SORS is a recently developed technique based on Raman spectroscopy that enables deep probing into translucent samples, such as biological tissues or powders, or through opaque barriers, such as plastic bottles or paper packaging,[5] in situations where the absorption scattering coefficient is negligible (i.e., in diffusion approximation[6,7]). This is often the case for SORS measurements carried out in the NIR spectral region, especially within the therapeutic window for biological tissues (650−950 nm), where it is possible to reach larger sampling depths[8,9] and, in fact, is an important prerequisite for effective SORS measurements in general. The ability to perform such measurements using existing SORS systems enriches researchers in possession of these instruments by enabling them, for example, to perform an effective optimization of the illumination and collection SORS geometry, to provide the key input parameters for Monte Carlo or other simulations of light propagation in turbid media, or to derive detailed information about the properties of SORS measurements such as probed depth.[10−12] Previous modeling of SORS geometries relied on the scattering coefficient to be derived from other measurements[10,13−16] (e.g., NIR diffuse reflectance in continuous wavelength,[17,18] frequency domain,[18] and time-resolved[19−21] approaches). A number of beneficiary fields include biomedical diagnostic[22−24] and therapeutic areas,[25−27] forensics,[28] pharmaceutical analysis,[29,30] explosives detection,[31] and analysis of objects in cultural heritage.[32,33]

The proposed concept relies on evaluating the decay of intensity of a selected Raman band with an increasing spatial offset between collection and illumination points. At least two distinct spatial offsets are required for the method (the zero spatial offset can be one of these). The rate of change of the

Received: October 12, 2020
Accepted: January 22, 2021
Published: February 11, 2021

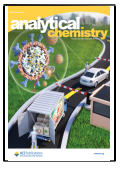

https://dx.doi.org/10.1021/acs.analchem.0c04290
Anal. Chem. 2021, 93, 3386−3392

Raman signal intensity with the spatial offset is strongly dependent on the medium's scattering coefficient, μ_s'. For a point-like collection and illumination SORS geometry, a larger scattering coefficient leads to a more rapid decay with spatial offset; conversely, a smaller μ_s' yields a shallower decay. As such, a fit analysis can be performed to find a matching μ_s', which produces the observed signal variation as a function of the spatial offset. It is the first time, to our knowledge, that this property is appreciated for its potential to be used to determine the scattering coefficient itself. Here we demonstrate this approach both theoretically and experimentally. The concept is closely related to spatially offset NIR diffuse scattering coefficient measurements with the exception that, in this case, the signal is converted (through the Raman process) to a different frequency.[34] This special feature provides an inherent advantage of the proposed methodology over conventional NIR methods, as it overcomes problems stemming from interference by specular reflection of the incoming probe radiation, an issue that complicates conventional NIR measurements where the detected radiation is identical in frequency to the incident one.[35] The Raman frequency shift enables effective filtering of the incident probe radiation. An additional assumption in the proposed methodology is that the reduced scattering coefficient is approximately the same for both the laser and the Raman line used to evaluate it. This represents a limitation of the proposed technique. Any measurement performed using this methodology yields a reduced scattering coefficient that is an average value of that at the laser and Raman frequency, since photon migration involves both the photons and as such the method is not suitable for samples with a strong dispersion of the scattering coefficient. However, the dispersion is not very strong, especially in many situations where NIR excitation is used in SORS studies, for example, with biological tissues.[36] Furthermore, this limitation can be mitigated by using a low wavenumber Raman band as a reference, so that the dispersion effect is minimized. It is also assumed that the sample is semi-infinite sideways and in depth, so that only the surface sample boundary is present.

NUMERICAL SIMULATIONS

To gain an insight into the proposed concept, we performed numerical simulations based on the Monte Carlo (MC) method.[37] Both elastically (laser) and nonelastically scattered (Raman) photons are individually followed as they propagate via a random walk through the medium in 3D space.[37,38] As in our previous MC simulations, a simplifying assumption is made such that the photon can travel along a straight line in each calculation step and, at the end of it, its direction is randomized. The traveled distance in each step is approximated by the transport length of the scattering medium, l_t.[39,40] The transport length is often significantly longer than the mean free path length, l_s , of the scattered photons in the medium. The precise relationship is $l_s = (1 - g)l_t$, where g is the anisotropy of the individual scattering events. In our analysis, we also assumed that the wavelength of light propagating through the medium is substantially shorter than the scattering path length l_s , which also holds true for most samples investigated by SORS in the relevant part of the spectrum.

The transport length is related to the reduced scattering coefficient of the medium through the relationship $l_t = 1/\mu_s'$. The model considers the sample to be a semi-infinite homogeneous turbid medium with an air−medium interface. As in our previous models,[38] we assumed that all the probe photons are first placed at a depth equal to the transport length l_t. The beam radius of the incident light is r, and the beam has a uniform intensity across it, that is, we assume it has a flat "top-hat" intensity profile, with all the photons having an equal probability of being injected into the sample at any point within its cross-section. At the code level, the overall propagation distance for each photon along with its collection coordinates are recorded as it emerges within the collection aperture of the Raman system. Since the probability of generating a Raman photon depends on the time that the probe photon spends within the medium (i.e., the propagation distance), then the probability of the photon being converted into a Raman photon during its overall path through the medium is proportional to the propagation distance. As we assume the transport length being the same for both the laser and the Raman frequency, the photon pathway is the same, irrespective of whether propagating as a laser or Raman photon. As such, for each "detected" photon, its propagation distance provides weighting that reflects the probability of it being converted into a Raman photon on its passage through the sample. These values are ultimately summed up for each spatial offset to express the overall likelihood of detecting Raman photons at that specific spatial offset. For maximum efficiency, to minimize noise stemming from the photon nature of signal detection (i.e., "photon shot" noise), the Raman light is collected in a SORS circular collection geometry through concentric annuli.[41,42] This maximizes the detected signal and minimizes the present calculation "photon shot" noise. This collection can be approximated in practice to a collection system consisting of an array of optical fibers, forming either a single annulus or a concentric set of annuli. Since the most illustrative and most common configuration is a point-like illumination and point-like collection SORS geometry, the data presented in this paper were converted into this geometry. Raman signal detected in a point-like collection geometry is derived from the calculated MC data by dividing the Raman signal detected through individual SORS annuli by the area of each specific annulus. It should be noted that general conclusions derived for point-like illumination and collection geometry in this paper are also valid by analogy for a point-like illumination and circular Raman collection geometry with negligibly thin annulus with respect to the transport length; and also holds for circular illumination and point-like collection geometry (inverse SORS) where both the Raman collection area dimension and illumination annulus thickness are smaller than the transport length under consideration.

The numerical code was written in Mathematica 9.0.1.0 (Wolfram Research). A total of 2000000 photons were propagated simultaneously, each over 10000 steps with a step size l_t varied in the range 0.2 to 2 mm. Unless stated otherwise, the basic conditions were as follows: the probe beam radius was $r = 1$ μm (approximating point illumination conditions) and the medium was assumed to be homogeneous and nonabsorbing. The photons were collected through 50 spatial offsets annuli of 0.2 mm width each, covering a range of spatial offsets from the illumination point ("zero spatial" offset) to 10 mm. The spatial offset, Δs, assigned to each annulus was defined as the radius at the center of the annulus (i.e., the arithmetic average of the annulus radii boundaries). The spatial offsets were purposely chosen to be small to facilitate the closest possible approximation to point-like illumination and

https://dx.doi.org/10.1021/acs.analchem.0c04290
Anal. Chem. 2021, 93, 3386−3392

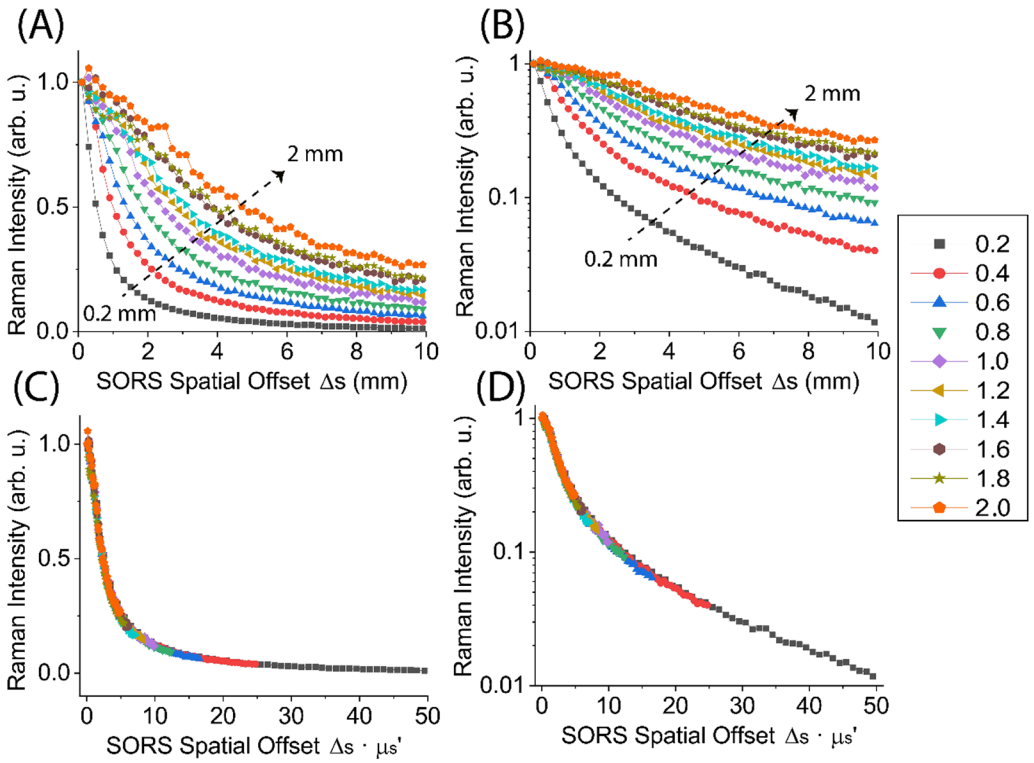

Figure 1. Raman intensity decay for point-like illumination and collection SORS geometry as a function of the SORS spatial offset (Δs) derived from Monte Carlo simulations shown in (a) linear and (b) logarithmic scales. The same data normalized to unitless spatial offset expressed as the product of SORS spatial offset and μ_s' shown in (c) linear and (d) logarithmic scales. The legend on the right applies to all the plots and indicates medium transport lengths in mm's.

point-like collection geometries derived from the calculated circular geometries.

The results of the MC calculations are shown in Figure 1A,B, which illustrates the above-mentioned strong dependence of the Raman signal decay with spatial offset on the reduced scattering coefficient μ_s'. It is evident that, knowing the relationship between the decay curve and μ_s' should enable μ_s' to be predicted from the curve of the Raman signal decay with spatial offset. The universality of the concept is emphasized by plotting the signal decay as a function of unitless spatial offset, expressed as the ratio of the spatial offset Δs and transport length (i.e., $\Delta s/l_t = \Delta s \cdot \mu_s'$). This illustrates that the curves collapse on top of each other in a master plot (Figure 1C,D), meaning that the problem becomes independent of the reduced scattering coefficient within the considered approximations. In other words, it is the transport length (or equally the reduced scattering coefficient) that defines the scale of the problem and, when all spatial variables are expressed as multiples of the transport length, a universal behavior is found. This can also be interpreted as evidence that the change in Raman signal with the reduced scattering coefficient for a point-like illumination and collection system is solely dependent on the reduced scattering coefficient, and no other parameter contributes to this dependence.

That is, if we had a point-like illumination and a point-like collection system, the dependencies would be identical for any system irrespective of whether operated on a microscale or macroscale under the above assumptions, as long as its spatial coordinates are expressed as multiples of the photon transport length l_t; in such a framework, all systems become identical and behave identically.

The universality of the signal decay in the unitless framework can be exploited by performing a fit analysis of the observed decay in Figure 1C,D by fitting the transport length l_t. This simple approach becomes, however, only an approximation when the SORS system is not made of a point-like illumination/collection and the size of either illumination or collection zone (or both) or, for example, the width of the Raman collection annulus in circular collection or illumination geometry become comparable or much larger than the transport length. However, even in this situation, any such system can be expressed as a superposition of point-like collection/illumination systems. To calculate the reduced scattering coefficient from the first-principles would, however, involve more complex fitting involving integration (or convolution if both the laser and Raman collection areas are nonpoint like) of signals from these individual point-like approximations to facilitate the appropriate fit. For such a system, rather than calculating the reduced scattering coefficient from the first-principles and using this value in the fit, we suggest calibrating the instrumental apparatus on a sample (or samples) with a known reduced scattering coefficient[43,44] to derive accurate values from the measurements of unknown samples. This approach is also adopted in this study.

EXPERIMENTAL SETUP

All Raman experiments were performed on a SORS system previously described.[45] In brief, we used a NIR laser with 830 nm wavelength and 200 mW power measured at the sample. The acquisition time was either 10 or 30 s with 6 or 4 accumulations, respectively. The laser illumination spot on the sample plane had a radius of 0.25 mm. The Raman signal from

https://dx.doi.org/10.1021/acs.analchem.0c04290
Anal. Chem. 2021, 93, 3386−3392

Table 1. Main Parameters and Measurement Settings of the Four Samples Used As Turbid Media

material	(x, y, z)	nominal data μ_s' (mm^{-1})	transport length, l_t (mm)	spatial offset, Δs (mm)	Raman bands	
					shift $\Delta\nu$ (cm^{-1})	λ (nm)
PTFE	50, 50, 12	1.0[a]	1.00	0, 2, 4, 6, 8, 10	291	850
					732	884
					1582	938
PE	50, 50, 15	0.6[a]	1.67	0, 2, 4, 6, 8, 10	1061	910
					1295	930
					1443	943
PS	50, 50, 10	1,7[a]	0.59	0, 2, 4, 6, 8, 10	620	875
					1001	905
					1183	920
ex vivo tissue	40, 40, 36	0.4[b]	2.50	0, 8, 10, 12, 14, 16	830	891
					1005	905
					1443	943

[a]The μ_s' values were derived from an average of the μ_s' coefficients measured using Time Domain Diffuse Optical Spectroscopy (TD-DOS)[43,46] in the same spectral range as the Raman measurements (830−970 nm). [b]For the ex vivo tissue, μ_s' was obtained in a similar way from another ex vivo porcine tissue analyzed previously.[36]

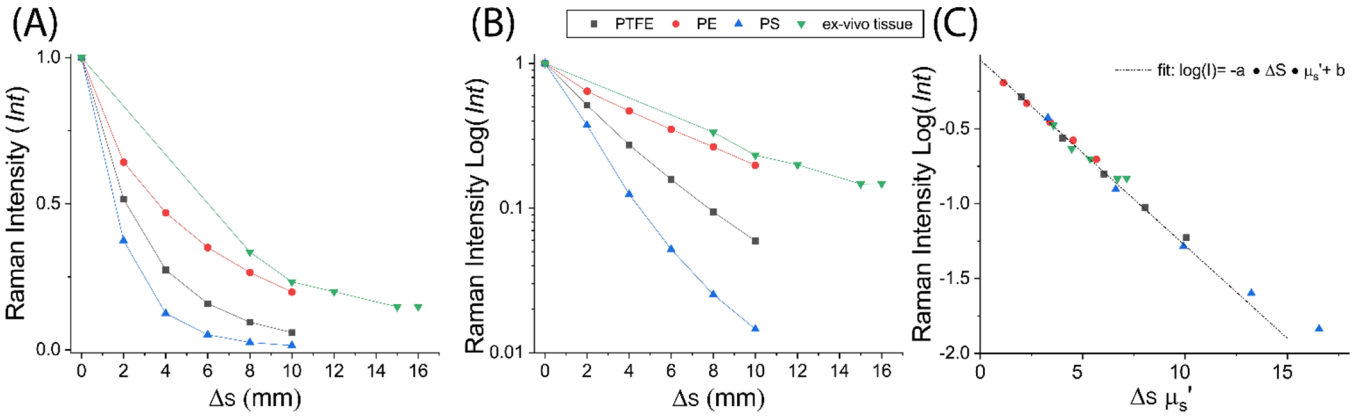

Figure 2. Raman intensity decays vs SORS spatial offset measured for the four model samples: (a) linear plot normalized to zero offset value and (b) log plot. (c) Log plot of the Raman intensity vs unitless $\Delta s \cdot \mu_s'$. Linear fit (black dotted line) of the PTFE data (black filled squares) show the calibration model used for the prediction of μ_s'.

the sample was collected in backscattering across an elongated spot, which can be approximated to a circle with 0.75 mm radius. The intensities of a number of intense Raman bands for each sample (see Table 1) were evaluated as the areas of the Gaussian curves were derived from a fit analysis of the peak for a given spatial offset.

SAMPLES

Four model samples were used as turbid media: polytetrafluoroethylene (PTFE), polyethylene (PE), polystyrene (PS), and semihomogeneous ex vivo porcine tissue. The main parameters of the model phantoms and related measurements are listed in Table 1.

CONCEPT VALIDATION

The dependence of the Raman intensity decay with spatial offset on the reduced scattering coefficient is numerically demonstrated in Figure 1, where Raman intensities are plotted as a function of spatial offset for turbid samples with different transport lengths ranging between 0.2 and 2.0 mm. Therefore, for a given system, knowing the decay profile of the SORS signal with spatial offset should yield the value of μ_s'. For example, the results of fitting the logarithmic dependence with the spatial offset shown in Figure. 1D are illustrated in Figure 2. The SORS system used in this study is not strictly point-like given the sizes of the illumination and collection areas (~0.25 mm and 0.75 mm in radius, respectively) with respect to the estimated transport lengths (~0.5−2.5 mm). Nevertheless, reasonably good fit results were obtained from purely theoretical calculations without any calibration, indicating that even such a nonperfect point-like system can be reasonably well approximated to a point-like one (see Figure SI1 in Supporting Information). The predicted average reduced scattering coefficient values were 1.2, 0.7, 2.6, and 0.49 mm^{-1} for PTFE, PE, PS, and the ex vivo tissue, respectively, were obtained this way from the first-principles without any calibration by matching the observed Raman signal decay to that derived from Monte Carlo simulations (see SI1).

However, as mentioned earlier, for a system departing more from the ideal point-like illumination/collection it would be safer to use calibration samples with known μ_s' to avoid the risk of potentially skewing the results. To demonstrate this, we carried out such calibration here. We used the same PTFE model sample for which we had derived the scattering coefficient from an earlier time- and space-resolved NIR diffuse reflectance study.[36] Figure 2 shows the experimental results for the four model samples. The decrease of Raman

https://dx.doi.org/10.1021/acs.analchem.0c04290
Anal. Chem. 2021, 93, 3386−3392

intensity as a function of the spatial offset (Figure 2A) resembles the decay obtained from the Monte Carlo simulation (see Figure 1). For a given system, this requires calibration with at least one sample of known μ_s', a calibration sample, here PTFE.

A calibration model for the prediction of μ_s' was developed as follows:

(i) For each SORS spatial offset (Δs = 0−10 mm), a Gaussian curve fit was performed on the Raman bands of PTFE (with known μ_s' from literature data) to quantitatively evaluate the intensity for each spatial offset (see Table 1).

(ii) All Raman intensity (Int) profiles for different values of spatial offset were normalized to the value measured at the zero spatial offset (Δs = 0 mm, Int = 1).

(iii) The decadic logarithm of the intensity against spatial offset multiplied by the reduced scattering coefficient ($\Delta s \cdot \mu_s'$) was linearly fit (Figure 2c).

(iv) The value of μ_s' ($\mu_s' = \frac{\log(\mathrm{Int}) - b}{a \cdot \Delta s}$, where a and b are free fitting parameters) was obtained as the average for all intensities and spatial offsets.

The achieved root-mean-square error of calibration (RMSEC) was 8.2% (0.075 mm^{-1}; Table 2).

Table 2. Average Predicted Value of the Reduced Scattering Coefficient Resulted from All the Spatial Offsets (mm^{-1}), Root-Mean-Square Error of Calibration (RMSEC for PTFE) and Prediction (RMSEP) for All the Model Samples Analyzed

material	average predicted μ_s' (mm^{-1})	RMSEC (mm^{-1})	RMSEC (%)
PTFE	1.08	0.075	8.3
material	average predicted μ_s' (mm^{-1})	RMSEP (mm^{-1})	RMSEP (%)
PE	0.63	0.055	9.8
PS	1.72	0.16	10.
ex vivo tissue	0.41	0.07	18.0

When the calibration data set is formed (steps (i)−(iii) on the PTFE sample), that is, the parameters a and b in the above formula are determined, one can predict μ_s' of an unknown sample. This is achieved by calculating the μ_s' using the above formula (step (iv) of the calibration procedure) with known parameters a and b and the collected intensities for the unknown sample (log (Int)) versus spatial offset. For each sample and each spatial offset, the values of μ_s' estimated from the intensities of different Raman bands of the sample were averaged in order to obtain a mean value of the reduced scattering coefficient in the near-infrared spectral range (850−900 nm). Figure 3 shows such a prediction of μ_s' values versus nominal values for various matrixes used in the study (PE, PS, and ex vivo tissues). The average μ_s' values (yellow stars in Figure 3) predicted from all the measured spatial offsets and different Raman bands are reported in Table 2. The proposed approach allowed the estimation of the scattering coefficient of turbid media with an error (RMSEP) below 18% (0.070 mm^{-1} for ex vivo tissue; Figure 3 and Table 2). These results validate the use of this approach for the estimation of the scattering coefficient of turbid media from the sole decay of Raman scattering intensity over spatial offset.

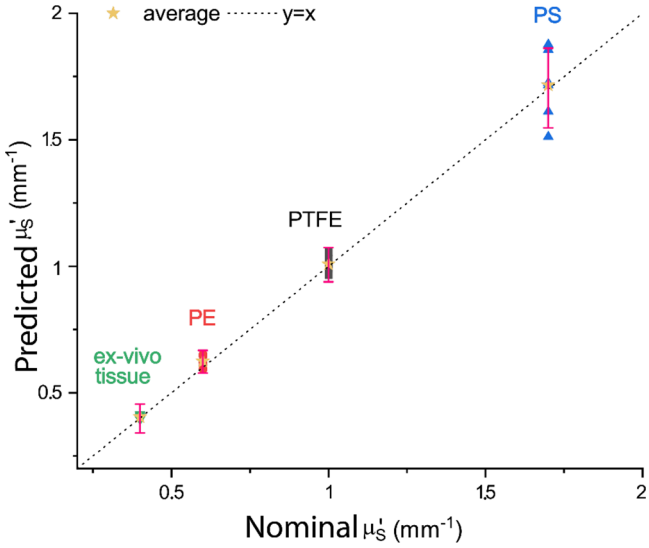

Figure 3. Plot of the predicted reduced scattering coefficients vs nominal values of four turbid samples using SORS. The yellow stars indicate the average value predicted from all spatial offsets. The system was calibrated on the PTFE values (black filled squares). Error bars (magenta) denote the average error of prediction.

CONCLUSION

We presented a new approach for estimating the value of transport length and reduced scattering coefficient μ_s' of turbid media using SORS in the approximation of ideal point-illumination/collection geometry. The methodology is valid for samples with negligible absorption and assumes that the reduced scattering coefficient is similar for the laser and Raman photon wavelengths. Further considerations related to the role of absorption are discussed in ref 12. The concept was validated on four different turbid samples, including biological tissue, with reduced scattering coefficient ranging from 0.3 to 2 mm^{-1}. The relative error of the estimated values was between 8% and 18%, the latter value plausibly reflecting spatial heterogeneity and residual water absorption in the tissue sample, as also suggested by the spread of data points for that sample. This approach provides a simple means for deriving reduced scattering coefficients using a SORS apparatus. This parameter can then be further employed in numerical simulations, which can aid SORS optimization and other photon propagation studies or to derive information about more detailed properties of SORS measurements.

ASSOCIATED CONTENT

Supporting Information

The Supporting Information is available free of charge at https://pubs.acs.org/doi/10.1021/acs.analchem.0c04290.

Monte Carlo simulation (intensity decay−fit), reduced scattering coefficient, and Raman spectrum of the model samples (PDF)

AUTHOR INFORMATION

Corresponding Authors

Nick Stone − *School of Physics and Astronomy, University of Exeter, Exeter EX4 4QL, United Kingdom;* orcid.org/0000-0001-5603-3731; Email: n.stone@exeter.ac.uk

Pavel Matousek − *Central Laser Facility, Research Complex at Harwell, STFC Rutherford Appleton Laboratory, UK*

https://dx.doi.org/10.1021/acs.analchem.0c04290
Anal. Chem. 2021, 93, 3386−3392

Research and Innovation, Didcot OX11 0QX, United Kingdom; orcid.org/0000-0003-0912-5339; Email: pavel.matousek@stfc.ac.uk

Authors

Sara Mosca − *Central Laser Facility, Research Complex at Harwell, STFC Rutherford Appleton Laboratory, UK Research and Innovation, Didcot OX11 0QX, United Kingdom;* orcid.org/0000-0001-9479-5614

Priyanka Dey − *School of Physics and Astronomy, University of Exeter, Exeter EX4 4QL, United Kingdom;* orcid.org/0000-0003-2896-7611

Marzieh Salimi − *School of Physics and Astronomy, University of Exeter, Exeter EX4 4QL, United Kingdom*

Benjamin Gardner − *School of Physics and Astronomy, University of Exeter, Exeter EX4 4QL, United Kingdom;* orcid.org/0000-0002-7223-9585

Francesca Palombo − *School of Physics and Astronomy, University of Exeter, Exeter EX4 4QL, United Kingdom;* orcid.org/0000-0001-6355-2601

Complete contact information is available at: https://pubs.acs.org/10.1021/acs.analchem.0c04290

Notes

The authors declare no competing financial interest.

■ ACKNOWLEDGMENTS

This work was supported by the Engineering and Physical Sciences Research Council Grant EP/R020965/1. The authors thank Pranav Lanka and Antonio Pifferi for support in the collection of the spectra of the reduced scattering coefficient shown in the Supporting Information SI2.

■ REFERENCES

(1) Alfano, R. R.; Wang, W. B.; Wang, L.; Gayen, S. K. In *Photonics*; Wiley, 2015; pp 367−412.
(2) Martelli, F.; Del Bianco, S.; Ismaelli, A.; Zaccanti, G. *Light Propagation through Biological Tissue and Other Diffusive Media: Theory, Solutions, and Software*; SPIE Press: Bellingham, Washington, U.S.A., 2010; pp 57−60.
(3) Contini, D.; Martelli, F.; Zaccanti, G. *Appl. Opt.* **1997**, *36* (19), 4587.
(4) Matousek, P.; Clark, I. P.; Draper, E. R. C.; Morris, M. D.; Goodship, A. E.; Everall, N.; Towrie, M.; Finney, W. F.; Parker, A. W. *Appl. Spectrosc.* **2005**, *59* (4), 393−400.
(5) Matousek, P. *TrAC, Trends Anal. Chem.* **2018**, *103*, 209−214.
(6) Martelli, F.; Contini, D.; Taddeucci, A.; Zaccanti, G. *Appl. Opt.* **1997**, *36* (19), 4600.
(7) Del Bianco, S.; Martelli, F.; Zaccanti, G. *Phys. Med. Biol.* **2002**, *47* (23), 4131−4144.
(8) Martelli, F.; Binzoni, T.; Pifferi, A.; Spinelli, L.; Farina, A.; Torricelli, A. *Sci. Rep.* **2016**, *6*, 1−14.
(9) Sekar, S. K. V.; Mosca, S.; Farina, A.; Martelli, F.; Taroni, P.; Valentini, G.; Cubeddu, R.; Pifferi, A. *Opt. Express* **2017**, *25* (5), 4585.
(10) Reble, C.; Gersonde, I.; Lieber, C. A.; Helfmann, J. *Biomed. Opt. Express* **2011**, *2* (3), 520.
(11) Mosca, S.; Dey, P.; Salimi, M.; Palombo, F.; Stone, N.; Matousek, P. *Analyst* **2020**, *145* (23), 7623−7629.
(12) Mosca, S.; Dey, P.; Marzieh, S.; Gardner, B.; Francesca, P.; Stone, N.; Matousek, P. Spatially Offset Raman Spectroscopy - How Deep? *Manuscript in preparation*, 2020.
(13) Keller, M. D.; Wilson, R. H.; Mycek, M.-A.; Mahadevan-Jansen, A. *Appl. Spectrosc.* **2010**, *64* (6), 607−614.
(14) Matousek, P.; Conti, C.; Colombo, C.; Realini, M. *Appl. Spectrosc.* **2015**, *69* (9), 1091−1095.
(15) Periyasamy, V.; Sil, S.; Dhal, G.; Ariese, F.; Umapathy, S.; Pramanik, M. *J. Raman Spectrosc.* **2015**, *46* (7), 669−676.
(16) Conti, C.; Botteon, A.; Colombo, C.; Realini, M.; Matousek, P. *Analyst* **2016**, *141*, 5374−5381.
(17) Zaccanti, G.; Del Bianco, S.; Martelli, F. *Appl. Opt.* **2003**, *42* (19), 4023.
(18) Pogue, B. W.; Patterson, M. S. *Phys. Med. Biol.* **1994**, *39*, 1157−1180.
(19) Spinelli, L.; Martelli, F.; Farina, A.; Pifferi, A.; Torricelli, A.; Cubeddu, R.; Zaccanti, G. *Opt. Express* **2007**, *15* (11), 6589.
(20) Bouchard, J.-P.; Veilleux, I.; Jedidi, R.; Noiseux, I.; Fortin, M.; Mermut, O. *Opt. Express* **2010**, *18* (11), 11495.
(21) Patterson, M. S.; Chance, B.; Wilson, B. C. *Appl. Opt.* **1989**, *28* (12), 2331−2336.
(22) Matousek, P.; Stone, N. *Chem. Soc. Rev.* **2016**, *45* (7), 1794−1802.
(23) Ntziachristos, V. *Nat. Methods* **2010**, *7* (8), 603−614.
(24) Demers, J.-L. H.; Esmonde-White, F. W. L.; Esmonde-White, K. A.; Morris, M. D.; Pogue, B. W. *Biomed. Opt. Express* **2015**, *6* (3), 793.
(25) Di Sieno, L.; Contini, D.; Lo Presti, G.; Cortese, L.; Mateo, T.; Rosinski, B.; Venturini, E.; Panizza, P.; Mora, M.; Aranda, G.; Squarcia, M.; Farina, A.; Durduran, T.; Taroni, P.; Pifferi, A.; Mora, A. D. *Biomed. Opt. Express* **2019**, *10* (8), 3899.
(26) Tabish, T. A.; Dey, P.; Mosca, S.; Salimi, M.; Palombo, F.; Matousek, P.; Stone, N. *Adv. Sci.* **2020**, *7* (15), 1903441.
(27) Liu, Y.; Zhang, C.; Wang, L. V. *J. Biomed. Opt.* **2012**, *17* (12), 126014.
(28) Macleod, N. A.; Matousek, P. *Pharm. Res.* **2008**, *25* (10), 2205−2215.
(29) Aina, A.; Hargreaves, M. D.; Matousek, P.; Burley, J. C. *Analyst* **2010**, *135* (9), 2328.
(30) Matousek, P.; Parker, A. W. *Appl. Spectrosc.* **2006**, *60* (12), 1353−1357.
(31) Eliasson, C.; Macleod, N. A.; Matousek, P. *Anal. Chem.* **2007**, *79* (21), 8185−8189.
(32) Botteon, A.; Colombo, C.; Realini, M.; Castiglioni, C.; Piccirillo, A.; Matousek, P.; Conti, C. *J. Raman Spectrosc.* **2020**, *51* (10), 2016−2021.
(33) Mosca, S.; Artesani, A.; Gulotta, D.; Nevin, A.; Goidanich, S.; Valentini, G.; Comelli, D. *Microchem. J.* **2017**, 1−6.
(34) Martelli, F.; Binzoni, T.; Sekar, S. K. V.; Farina, A.; Cavalieri, S.; Pifferi, A. *Opt. Express* **2016**, *24* (18), 20382.
(35) Hanssen, L. M.; Snail, K. A. In *Handbook of Vibrational Spectroscopy*; Griffiths, P. R., Ed.; John Wiley & Sons, Ltd.: Chichester, U.K., 2001.
(36) Mosca, S.; Lanka, S. R. P. K.; Stone, N.; Valentini, G.; Konugolu Venkata Sekar, S.; Matousek, P.; Pifferi, A. *Biomed. Opt. Express* **2020**, *11* (3), 1697−1706.
(37) Jacques, S. L.; Wang, L. *Optical-Thermal Response of Laser-Irradiated Tissue. Lasers, Photonics, and Electro-Optics*; Springer: Boston, MA, 1995; pp 73−100.
(38) Matousek, P.; Morris, M. D.; Everall, N.; Clark, I. P.; Towrie, M.; Draper, E.; Goodship, A.; Parker, A. W. *Appl. Spectrosc.* **2005**, *59*, 1485−1492.
(39) Brenan, C. J. H.; Hunter, I. W. *J. Raman Spectrosc.* **1996**, *27* (8), 561−570.
(40) Das, B. B.; Liu, F.; Alfano, R. R. *Rep. Prog. Phys.* **1997**, *60*, 227−292.
(41) Corden, C.; Matousek, P.; Conti, C.; Notingher, I. *Appl. Spectrosc.* **2020**, DOI: 10.1177/0003702820946054.
(42) Nicolson, F.; Kircher, M. F.; Stone, N.; Matousek, P. *Chem. Soc. Rev.* **2021**, *50*, 556−568.
(43) Sekar, S. K. V.; Pacheco, A.; Martella, P.; Li, H.; Lanka, P.; Pifferi, A.; Andersson-Engels, S. *Biomed. Opt. Express* **2019**, *10* (4), 2090.
(44) Vardaki, M. Z.; Kourkoumelis, N. *Biomed. Eng. Comput. Biol.* **2020**, *11*, 1−15.

(45) Mosca, S.; Dey, P.; Tabish, T. A.; Palombo, F.; Stone, N.; Matousek, P. *Anal. Chem.* **2019**, *91*, 8994−9000.
(46) Martelli, F.; Del Bianco, S.; Zaccanti, G.; Pifferi, A.; Torricelli, A.; Bassi, A.; Taroni, P.; Cubeddu, R. *Opt. Lett.* **2004**, *29* (17), 2037.

https://dx.doi.org/10.1021/acs.analchem.0c04290
Anal. Chem. 2021, 93, 3386−3392